Imaginary branches of surface acoustic wave slowness curves

Vincent Laude[a)]
Département LPMO, Institut FEMTO-ST, Centre National de la Recherche Scientifique UMR 6174, F-25044 Besancon cedex, France

Mathias Masson
Material Physics Laboratory, Helsinki University of Technology, P.O. Box 2200 FIN-02015 HUT, Finland

Sylvain Ballandras
Département LPMO, Institut FEMTO-ST, Centre National de la Recherche Scientifique UMR 6174, F-25044 Besancon cedex, France

Marc Solal
Temex, 399 route des Cretes BP 232 06904 Sophia Antipolis, France

(Received 18 June 2004; accepted 17 September 2004)

The imaginary branches of surface acoustic wave slowness curves are needed in many modal or spectral models that account for waveguides or diffraction based on the angular spectrum of waves approach. Their determination for an arbitrary anisotropic piezoelectric substrate considering either free or shorted surface boundary conditions is discussed. In the case of true, i.e., lossless, surface acoustic wave, the imaginary branches are obtained by a search in the complex transverse slowness plane as a function of the propagation slowness. As a side result, the parabolic approximation is compared with the exact solution and it turns out that its quality depends dramatically on the particular material cut considered. The case of pseudo- or leaky surface acoustic waves is also analyzed and it is found that difficulties arise in connection with the partial-wave selection rule for semi-infinite substrates. © *2004 American Institute of Physics*. [DOI: 10.1063/1.1813639]

I. INTRODUCTION

The study of waveguides by modal methods is based on expansions on partial waves, which are obtained by solving for plane waves in the different regions of the waveguide.[1,2] This general procedure is closely related to diffraction analysis by the angular spectrum of waves approach.[3] In the context of surface acoustic waves (SAW), the prediction of diffraction has motivated numerous studies, usually in view of identifying transducer or filter structures minimizing their adverse effects.[4–6] Waveguiding effects have been used for various applications, including filter structures taking advantage of the coupling between waveguides.[7–9]

Straight-crested (SC) acoustic surface waves have real-valued components of their wave vector in the plane of the surface. This type of surface wave is the most commonly considered. Slowness curves can be obtained for them using well-established methods.[10,11] Among partial waves occurring in waveguide or diffraction analysis, some are of the SC type, but others have an evanescent, or more generally inhomogeneous, dependence along the direction transverse to the propagation direction. We refer to them as laterally evanescent (LE) surface waves. The wave vectors of LE partial waves have one or more complex valued components. While the slowness of SC partial waves is given by slowness curves, LE partial waves lie on imaginary branches of these slowness curves.

In the case of isotropic propagation, the SAW slowness curves are circles and the imaginary branches of slowness curves are easily obtained analytically as radical functions. However, piezoelectric materials are necessarily anisotropic, and the slowness curves cannot, in general, be represented in a form suitable for the analytical expression of their imaginary branches. The usual procedure is then to use an approximation to the slowness curve known as the parabolic approximation,[12,13] from which the imaginary branches can be obtained analytically, as summarized in Sec. II. When the parabolic approximation is not valid, the analysis cannot be conducted further.

The purpose of this work is to obtain directly the imaginary branches of SAW slowness curves by formulating a plane-wave propagation problem with a complex transverse slowness, as explained in Sec. III. It is expected that this will lead to an improvement of the many modal or spectral methods that have been developed to account for waveguides or diffraction, with the imaginary branches of slowness curves being exact instead of the result of the parabolic or another approximation. As a side result, the parabolic approximation will be compared with the exact solution.

In the case of true, i.e., lossless, SAW, it will be shown in Sec. IV that the imaginary branches can be obtained by a search in the complex transverse slowness plane as a function of the propagation slowness. This case includes the Rayleigh SAW. When trying to extend the method to pseudo- or leaky SAW (PSAW) in Sec. V, difficulties will arise as regards the identification of a solution. These difficulties are twofold, with possible problems of partial-waves selection or the appearance of amplification rather than attenuation of SAW in the effective permittivity computation.

[a)]Electronic mail: vincent.laude@lpmo.edu

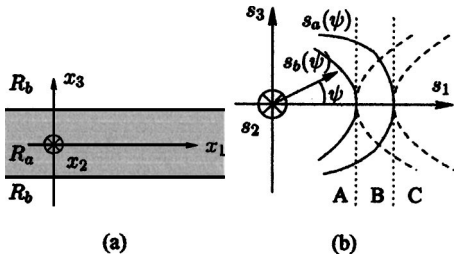

FIG. 1. (a) A simple symmetric strip SAW waveguide on a piezoelectric substrate and (b) a sketch of the slowness curves for straight-crested SAW (solid line) in regions R_a and R_b of the waveguide together with the corresponding imaginary branches for laterally evanescent SAW propagating along axis x_1 (dashed line).

II. DEFINITIONS

A generic example of a waveguiding structure for which a partial-wave expansion is useful is depicted in Fig. 1(a). This structure is a simple model for a strip waveguide. The symmetric structure is composed of a central region, R_a, surrounded by two semi-infinite regions, R_b. In both regions, the propagation of surface acoustic waves is assumed nondispersive but anisotropic. The particular slowness curves for SC surface waves in regions R_a and R_b are sketched in Fig. 1(b). It is assumed that the slowness is larger in region R_a than in region R_b since otherwise the structure would not guide waves. The partial waves in each homogeneous region are taken to be harmonic plane-wave solutions of the form

$$f(x_2)\exp[j\omega(t - s_1x_1 - s_3x_3)], \tag{1}$$

where ω is the angular frequency. The space coordinates of an observation point are (x_1, x_2, x_3), and (s_1, s_2, s_3) are the components of the slowness vectors. Axis x_1 is the propagation direction, axis x_2 enters the substrate, and axis x_3 is the transverse direction. The dependence on x_2 is not explicitly specified at this point, but it should be kept in mind that Eq. (1) represents a surface acoustic wave, so that $f(x_2)$ expresses the evanescent character of the amplitudes of the wave far from the surface. This dependence will be obtained from the surface boundary conditions. In a modal description of the waveguide, the component of the slowness vector along the waveguide axis, s_1, is a real valued parameter specifying the phase velocity of the particular mode for a given angular frequency ω. For the geometry of Fig. 1(a), the phase-matching condition imposes that s_1 be the same in regions R_a and R_b. s_3 in each region is then obtained by satisfying the dispersion relation for SAW. The slowness curves for SC partial waves can be obtained by setting

$$s_1 = s(\psi)\cos(\psi),$$

$$s_3 = s(\psi)\sin(\psi), \tag{2}$$

where ψ is the propagation angle in the plane of the surface, and by solving for the slowness modulus s as a function of ψ. In the (s_1, s_3) plane of Fig. 1(b) there appears three possible situations labeled A, B, and C according to whether there exist or not SC surface waves in regions R_a and R_b as s_1 is varied. In situation A, there exist, SC surface waves in both the central region and the surrounding surface, and true waveguiding is not possible since elastic energy is not constrained to remain within the waveguide. A proper treatment of this situation requires the concept of a continuum of radiated modes as was shown in the context of dielectric optical waveguides[2] and of SAW laterally coupled waveguides.[8] In situation B, SC surface waves exist in the central region but not over the surrounding surface, where there exist LE SAW instead, i.e., SAW amplitudes are necessarily decreasing away from the central region. This is the waveguiding situation for which elastic energy cannot escape from the central region. Lateral boundary conditions at the transition from region R_a to R_b can normally be written and will result in the fact that only a discrete number of guided modes can exist.[1,2] These lateral boundary conditions for SAW are usually based on a scalar potential theory.[8,9,14] In region C, only LE surface waves propagate in the central region and the surrounding surface. However, no guided mode can be constructed from only LE partial waves, as discussed in Ref. 1. In the rest of this paper, we are interested in situation B and in obtaining the imaginary branches giving the complex-valued s_3 as a function of the real-valued s_1.

If propagation is isotropic in the plane of the surface, then the SAW slowness curve is a circle with equation

$$s_1^2 + s_3^2 = S^2, \tag{3}$$

where S is a constant slowness. This situation is, for instance, representative of C-axis-oriented hexagonal piezoelectric media, such as aluminum nitride. If $s_1 \leqslant S$, i.e., for SC surface waves, then s_3 can be expressed as a function of s_1 as the radical $\pm\sqrt{S^2 - s_1^2}$, which defines two real branches of the slowness curve. If $s_1 > S$, i.e., for LE surface waves, then $s_3(s_1) = \pm j\sqrt{s_1^2 - S^2}$ becomes purely imaginary, which defines two imaginary branches of the slowness curve. The choice of the imaginary branch depends on the sign of x_3 and is made so that the partial wave is transversally evanescent but never increasing.

In the general case of anisotropic propagation in the plane of the surface, it is not, in general, possible to obtain a direct exact relation between s_1 and s_3 such as Eq. (3). The parabolic approximation is often used with anisotropic materials because it leads to such a simple relationship. Despite its name, this approximation is that the slowness curve for small s_3 is an ellipse of equation

$$s_1^2 + (1 + \Gamma)s_3^2 = S^2, \tag{4}$$

where Γ is a constant parameter measuring the local departure of the slowness curve from a circle.[15] S is again a constant slowness. The approximation of Eq. (4) is only valid around the point $s_1 = S$ and $s_3 = 0$. We assume for simplicity in the following derivation that $1 + \Gamma > 0$. The two real branches of the slowness curve are given similarly to the isotropic case by

$$s_3(s_1) = \pm \frac{\sqrt{S^2 - s_1^2}}{\sqrt{1 + \Gamma}}, \tag{5}$$

while the two imaginary branches for propagation along the x_1 axis are given by

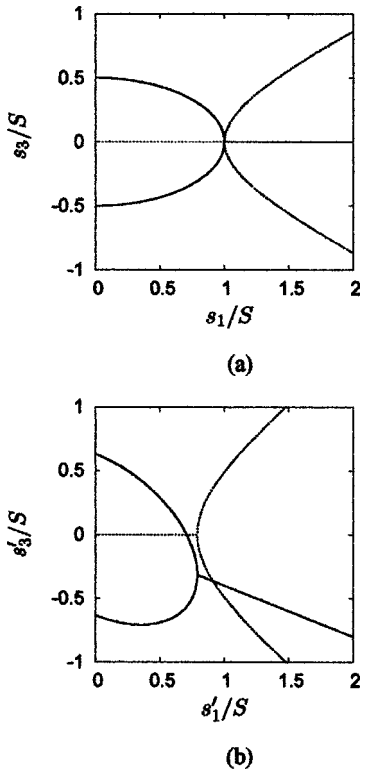

FIG. 2. Real (solid line) and imaginary (dotted line) branches in the frame of the parabolic approximation with $\Gamma=3$. (a) Propagation along the x_1 axis and (b) along axis x_1' which is obtained by a $-\pi/$four rotation of axis x_1 in the plane of the surface.

$$s_3(s_1) = \pm j\frac{\sqrt{{s_1}^2 - S^2}}{\sqrt{1+\Gamma}}. \tag{6}$$

Figure 2(a) displays the real and imaginary branches of Eqs. (5) and (6) for $\Gamma=3$. We emphasize that there is one fundamental difference between the real and imaginary branches of slowness curves. Real branches are essentially a remapping of the parametric slowness curve of Eq. (2); if the reference frame (x_1, x_3) of the surface is rotated by an angle ψ, then the real branches are readily obtained by rotating the slowness curve by an angle $-\psi$ in the (s_1, s_3) plane. The imaginary branches, however, are dependent on the propagation axis x_1. In order to show explicitly this dependence, let us consider the propagation along axis x_1' which is the image of axis x_1 in a rotation of angle ψ. Defining (s_1', s_3') as the $-\psi$ rotated slowness axes, the ellipse of Eq. (4) becomes

$$(1+\Gamma\sin^2\psi)(s_1')^2 + (1+\Gamma\cos^2\psi)(s_3')^2 + \Gamma\sin(2\psi)s_1's_3' = S^2. \tag{7}$$

The branch point between the real and imaginary branches is given by

$$(s_1')_B = \sqrt{\frac{1+\Gamma\cos^2\psi}{1+\Gamma}}S, \tag{8}$$

$$(s_3')_B = \frac{-\Gamma\sin(2\psi)}{2\sqrt{1+\Gamma}\sqrt{1+\Gamma\cos^2\psi}}S. \tag{9}$$

Before the branch point, i.e., for $s_1 < (s_1')_B$, the real branches are obtained as

$$s_3'(s_1') = \frac{-\Gamma\sin(2\psi)s_1'/2 \pm \sqrt{1+\Gamma}\sqrt{{(s_1')_B}^2 - (s_1')^2}}{1+\Gamma\cos^2\psi}, \tag{10}$$

while after the branch point, i.e., for $s_1 > (s_1')_B$, the imaginary branches are given by

$$s_3'(s_1') = \frac{-\Gamma\sin(2\psi)s_1'/2 \pm j\sqrt{1+\Gamma}\sqrt{(s_1')^2 - {(s_1')_B}^2}}{1+\Gamma\cos^2\psi}. \tag{11}$$

The real and imaginary branches of Eqs. (10) and (11) are displayed in Fig. 2(b) for $\Gamma=3$ and a rotation angle $\psi=\pi/4$. By the way, it is apparent that the imaginary branches can include a real part whenever $s_1(\psi)$ on the slowness curve is not maximal for $\psi=0$, that is when the branch point is not on axis.

III. METHOD OF SOLUTION

We next describe a method to obtain the imaginary branches of SAW slowness curves that is valid for arbitrary piezoelectric substrates without resorting to an approximation. The method is an extrapolation of the usual procedures to find SAW slowness curves.

We start by summarizing the well-known partial-waves theory for piezoelectric materials.[16] Propagation of plane surface acoustic waves with angular frequency ω is considered in the (x_1, x_3) plane, with slownesses s_1 and s_3. Assuming a plane-wave propagation, the distribution of the electromechanical fields in a piezoelectric material is fully described[16,17] using the eight-component state vector $\mathbf{h}=(u_1,u_2,u_3,\phi,T_{21},T_{22},T_{23},D_2)^t$, where the u_i are the mechanical displacements, ϕ is the electrical potential, T_{ij} is the stress tensor, and D_2 is the electrical displacement normal to the propagation surface. This state vector is obtained as a superposition of eight partial waves, characterized by their eigenvalues $s_2(n)$ and their associated eigenvectors, for $n=1,\ldots,8$. The eigenvalues $s_2(n)$ only depend on the material constants and on the slownesses s_1 and s_3. Denoting by F the 8×8 matrix of the vertically arranged eigenvectors, this superposition reads

$$\mathbf{h}(x_1,x_2,x_3) = F\Delta(x_2)\mathbf{a}\exp[j\omega(t - s_1x_1 - s_3x_3)], \tag{12}$$

where the dependence of the fields along axis x_2 is contained in the 8×8 diagonal matrix $\Delta(x_2)$ whose elements are

$$\Delta_{nn}(x_2) = \exp[-j\omega s_2(n)x_2]. \tag{13}$$

$\mathbf{a}$ is the vector of the eight amplitudes of the partial waves, whose values are obtained when the boundary conditions are specified. To account for the permittivity of vacuum above the substrate, the eight line of matrix F is modified according to[18]

$$F(8,i) \leftarrow F(8,i) + j\epsilon_0\sqrt{{s_1}^2 + {s_3}^2}F(4,i), i = 1,\ldots,8. \tag{14}$$

The matrix F of eigenvectors can also be written as

$$F = \begin{pmatrix} \mathcal{U} \\ \Phi \\ \mathcal{T} \\ \mathcal{D} \end{pmatrix}, \tag{15}$$

$\mathcal{U}$ and $\mathcal{T}$ are 3×8 matrices containing, respectively, the displacements and the normal constraints parts of the eigenvectors. Φ and $\mathcal{D}$ are 1×8 matrices containing, respectively, the potential and the normal electrical displacement parts of the eigenvectors.

Because we are considering a semi-infinite substrate supporting the propagation of SAW, not all partial waves are acceptable solutions. When both s_1 and s_3 are real, the partial-wave selection rule is well established.[19] Partial waves for which s_2 is real are acceptable if the component along axis x_2 of their Poynting vector enters the substrate; otherwise, if s_2 is complex, only if its imaginary part is positive can the partial wave be selected. Acceptable partial waves are referred to as reflected partial waves in analogy to the problem of reflection of acoustic waves on the surface of the substrate. By opposition, nonacceptable partial waves are termed transmitted. It turns out that the selection rule always results in four reflected (selected) and four transmitted (rejected) partial waves. The issue of partial-wave selection when s_1 is considered complex to account for attenuation is still a subject of controversy in the context of PSAW.[20] This case, however, will not be considered here. s_3 is here allowed to become complex to describe transversally inhomogeneous waves, not attenuated waves. Nevertheless, it should be verified that a meaningful partial-wave selection can be performed. This discussion is deferred to Sec. V; we will assume in the rest of this section that four reflected partial waves have been selected and that the matrix F and its submatrices $\mathcal{U}$, $\mathcal{T}$, Φ, and $\mathcal{D}$ have been restricted to the corresponding four eigenvectors.

Surface wave solutions must satisfy the surface boundary conditions. As is usual, we consider either free or shorted boundary conditions. In both cases, the normal mechanical constraints must vanish. In the case of the free surface, the normal electrical displacement is continuous across the surface, while in the case of the shorted surface, the potential vanishes on the surface. Using these definitions with the superposition of Eq. (12), it is readily found that the free boundary conditions are satisfied only if the following 4×4 determinant vanishes:

$$\Delta_F(s_1,s_3) = \begin{vmatrix} \mathcal{T} \\ \mathcal{D} \end{vmatrix}. \tag{16}$$

Conversely, the shorted boundary conditions are satisfied only if the following 4×4 determinant vanishes:

$$\Delta_S(s_1,s_3) = \begin{vmatrix} \mathcal{T} \\ \Phi \end{vmatrix}. \tag{17}$$

In Eqs. (16) and (17), the dependence of the determinants upon the surface slownesses has been explicitly indicated. The effective permittivity is related to these determinants through

$$\epsilon_{\text{eff}}(s_1,s_3) = \frac{\Delta_F(s_1,s_3)}{j|s_1|\Delta_S(s_1,s_3)}. \tag{18}$$

Finding the SC SAW slowness curves for the free and the shorted boundary conditions then amounts to locating the zeros of the determinants Δ_F and Δ_S. More precisely, the polar coordinates of Eq. (2) are used, and for every value of ψ, the slowness modulus $s(\psi)$ is adjusted so that the determinant vanishes. Finding the imaginary branches for LE SAW is a relatively similar procedure. For every real value of s_1 above the branch point [defined by the angle ψ that maximizes $s(\psi)\cos(\psi)$], a zero of the determinant is searched

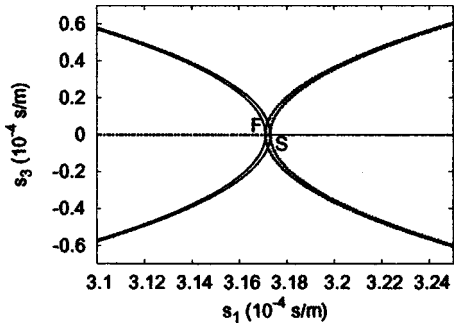

FIG. 3. Slowness curves (thick solid line) and their imaginary branches for propagation along axis x_1 (thick dashed line) for (YXl)/36 quartz and for both free (F) and shorted (S) boundary conditions. The parabolic approximation (thin dashed line) is almost indistinguishable from the real and imaginary branches.

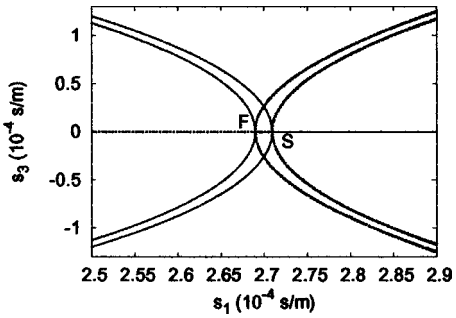

FIG. 4. Slowness curves (thick solid line) and their imaginary branches for propagation along axis x_1 (thick dashed line) for (YX) lithium niobate and for both free (F) and shorted (S) boundary conditions. The parabolic approximation (thin dashed line) is almost indistinguishable from the real and imaginary branches.

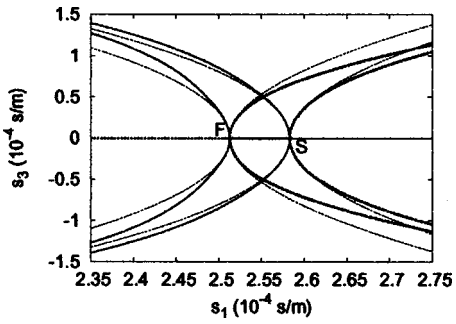

FIG. 5. Slowness curves (thick solid line) and their imaginary branches for propagation along axis x_1 (thick dashed line) for (YXl)/128 lithium niobate, and for both free (F) and shorted (S) boundary conditions. The parabolic approximation (thin dashed line) is also shown.

TABLE I. Parameters for the parabolic approximation. LN: lithium niobate; BC: boundary condition.

Material cut	BC	S (10^{-4} s/m)	Γ
(YXl)/36 quartz	free	3.1710	0.370
	shorted	3.1730	0.369
(YX) LN	free	2.6897	−0.232
	shorted	2.7092	−0.235
(YXl)/128 LN	free	2.5129	−0.339
	shorted	2.5831	−0.343
(YZ) LN	free	2.8674	−0.798
	shorted	2.9317	−0.513

for by varying s_3 in the complex plane. Since the transition from the real branches to the imaginary branches must be continuous, the branch point is a natural starting point for the algorithm. Because the determinants of Eqs. (16) and (17) are analytic functions of the complex slowness s_3, as long as the partial-wave selection rule is continuous, efficient algorithms can be used for finding the roots in the complex plane. Examples of imaginary branches are given in the next section.

IV. RESULTS FOR SURFACE ACOUSTIC WAVES

Figures 3–5 show the slowness curves and their imaginary branches for propagation along axis x_1, for (YXl)/36 quartz, (XY) lithium niobate (LN), and (YXl)/128 LN, respectively. Material cuts are given according to the IEEE 1949 standard. For Figs. 3–5, propagation characteristics are symmetrical with respect to the x_1 axis, so that the branch point is on axis. The parabolic approximation is also shown for comparison, with the parameters given in Table I. These parameters have been estimated directly from the slowness curve. It can be observed that the parabolic approximation is accurate for both (YXl)/36 quartz and (XY) LN over a large range of s_3, but over a smaller range for (YXl)/128 LN.

Figure 6 shows the slowness curve and its imaginary branches for propagation along axis x_1 for (XYt)/112.2 lithium tantalate (LT). For this material cut, propagation characteristics are not symmetrical with respect to the x_1 axis, so that the branch point is not on the x_1 axis. It can be observed that the imaginary branches possess a nonzero real part, as in the case of the rotated ellipse of Fig. 2(b). A further inspection, however, indicates that it cannot be approximated by a rotated ellipse; hence, the parabolic approximation as defined in Sec. II cannot be employed in this case.

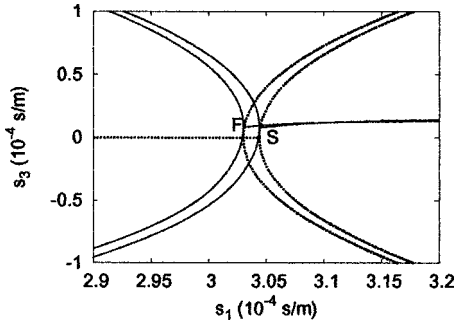

FIG. 6. Slowness curves (thick solid line) and their imaginary branches for propagation along axis x_1 (thick dashed line) for (XYt)/112.2 lithium tantalate and for both free (F) and shorted (S) boundary conditions.

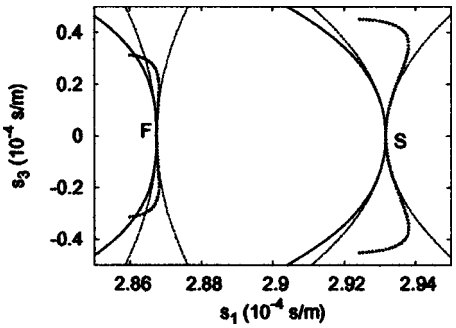

FIG. 7. Slowness curves (thick solid line) and their imaginary branches for propagation along axis x_1 (thick dashed line) for (YZ) lithium niobate and for both free (F) and shorted (S) boundary conditions. The parabolic approximation (thin dashed line) is also shown.

Figure 7 shows the slowness curve and its imaginary branches for propagation along axis x_1 for (YZ) LN. Though the slowness curves are symmetrical with respect to the x_1 axis, the imaginary branches show a peculiar behavior; they first exhibit a concavity as predicted by the parabolic approximation, but are then curving back towards decreasing s_1. As a result, there is a range of s_1 values for which both straight-crested and laterally evanescent SAW solutions can exist simultaneously.

V. CASE OF PSEUDO-SURFACE ACOUSTIC WAVES

As discussed in Ref. 20, the representation of the attenuation of PSAW by complex values of s_1, with $s_3=0$, can lead to a discontinuity in the partial-wave selection rule. It is then legitimate to wonder whether this is also the case when s_3 is allowed to become complex, with s_1 real, to generate imaginary branches of slowness curves, as in the present work. We will only discuss this problem in the context of slowness curves that are such that the branch point between the real and imaginary branches of SAW slowness curves lies on axis. This is the standard case of Y-rotated cuts of LT and LN. As argued above, in this case, purely imaginary branches are obtained for propagation along axis x_1. We then find it useful to explore the Π_{13} plane, defined as the (s_1, s_3) plane, with s_1 purely real and s_3 purely imaginary. Two tests are performed for each point in this plane. First, it is verified that a meaningful partial-wave selection can be performed. We

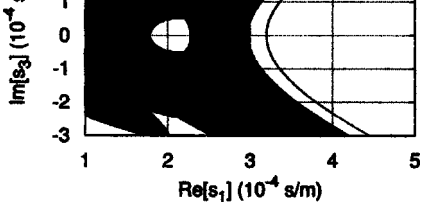

FIG. 8. Locus of initially allowed (in white) vs nonallowed (in black) LE SAW solutions in the Π_{13} plane for (YXl)/36 lithium tantalate. The imaginary branches of the slowness curve for Rayleigh-SAW propagating along axis x_1 are also shown.

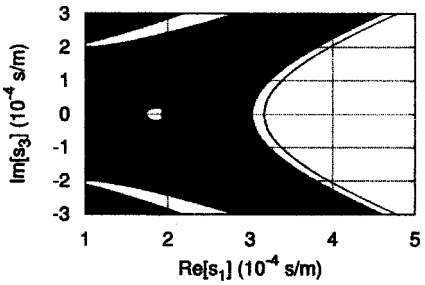

FIG. 9. Locus of initially allowed (in white) vs nonallowed (in black) LE SAW solutions in the Π_{13} plane for (YXl)/36 quartz. The imaginary branches of the SAW slowness curve for propagation along axis x_1 are also shown (they appear also in Fig. 3).

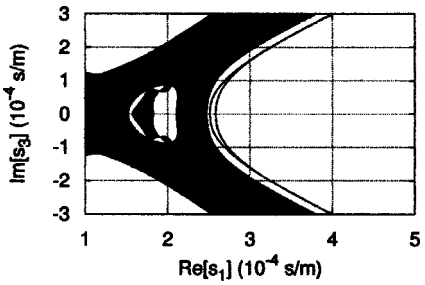

FIG. 11. Locus of initially allowed (in white) vs nonallowed (in black) LE SAW solutions in the Π_{13} plane for (YXl)/128 lithium niobate. The imaginary branches of the SAW slowness curve for propagation along axis x_1 are also shown (they appear also in Fig. 5).

observe numerically that there is a possibility that the partial waves be separated in a group of three reflected and a group of five transmitted partial waves, or the converse situation, depending on the sign of the imaginary part of s_3. A simple example of a slowness curve exhibiting this property is discussed analytically in the Appendix. As explained in Sec. III, the normal situation is the equipartition of reflected and transmitted partial waves. Furthermore, the determinants of surface boundary conditions, Eqs. (16) and (17), require four partial waves exactly. If this is not the case, the theory presented in this paper is unable to yield a solution. Second, the effective permittivity, as defined by Eq. (18), is computed and it is verified that its imaginary part is either negative or zero. When the imaginary part of the effective permittivity is positive, this is an indication that amplification of SAW is taking place instead of attenuation, which is not acceptable for a meaningful solution. In the following, we will refer as initially allowed LE SAW solutions to those point of the Π_{13} plane for which both tests succeed. Conversely, for initially not allowed LE SAW solutions, at least one of the tests fails.

Figure 8 displays the locus of initially allowed (in white) and not allowed (in black) LE SAW solutions in the Π_{13} plane for (YXl)/36 LT. Also, though this is hardly apparent on the figure, points on axis s_1 are always initially allowed. The pseudo- or leaky SAW of (YXl)/36 LT is widely used for radio-frequency SAW devices. There is also a Rayleigh SAW which is seldom used in practice because of its small electromechanical coupling coefficient. The imaginary branches of the slowness curves of the Rayleigh SAW for propagation along axis x_1, also shown in Fig. 8, are seen to be entirely within the initially allowed region. In contrast, the imaginary branches of the PSAW for free and shorted boundary conditions, originating from the s_1 axis at $s_1 = 2.4\ 10^{-4}$ s/m approximately, almost immediately encounter the initially not allowed region as $|s_3|$ increases from zero. The method described in Sec. III is thus unable to generate these imaginary branches. The situation has been verified to be similar with others common PSAW cuts such as (YXl)/42 LT, (YXl)/41 LN, and (YXl)/64 LN.

As a further numerical verification, we have plotted loci similar to that of Fig. 8 for the material cuts of Sec. IV. These are shown in Figs. 9–12 for (YXl)/36 quartz, (YX) LN, (YXl)/128 LN, and (YZ) LN, respectively. The imaginary branches of SAW slowness curves with free and shorted surface boundary conditions, appearing in Figs. 3–5 and 7, are also shown on the graphs. As for (YXl)/36 LT, the imaginary branches of the SAW slowness curves are seen to be entirely inside the respective initially allowed regions. In the particular case of (YZ) LN, Fig. 12, the abrupt endings of the imaginary branches occur when the initially nonallowed region is reached.

VI. CASE OF A FINITE-THICKNESS METALLIZATION

The previous discussion has been limited to a semi-infinite piezoelectric substrate with either free or shorted boundary conditions. In this section, the case of a finite thickness metallization is considered. The algorithms of Sec. III are straightforwardly generalized by replacing the surface effective permittivity of Eq. (18) by the interface effective permittivity[18,21] relating surface charges to the potential at the interface between piezoelectric and metal. The slowness

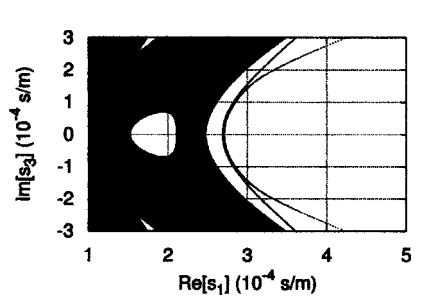

FIG. 10. Locus of initially allowed (in white) vs nonallowed (in black) LE SAW solutions in the Π_{13} plane for (YX) lithium niobate. The imaginary branches of the SAW slowness curve for propagation along axis x_1 are also shown (they appear also in Fig. 4).

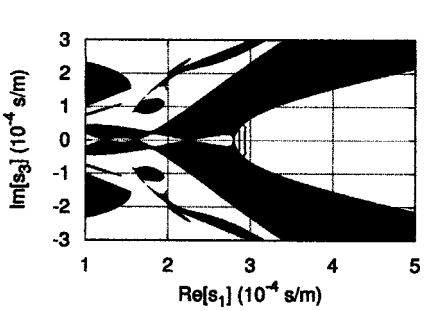

FIG. 12. Locus of initially allowed (in white) vs nonallowed (in black) LE SAW solutions in the Π_{13} plane for (YZ) lithium niobate. The imaginary branches of the SAW slowness curve for propagation along axis x_1 are also shown (they appear also in Fig. 7).

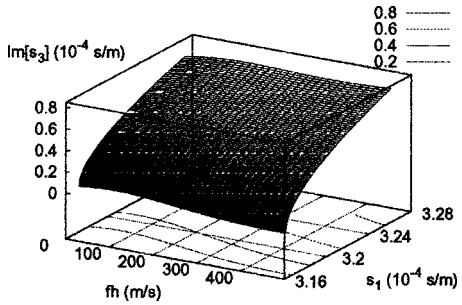

FIG. 13. Imaginary branches of the SAW slowness curves of (YXl)/36 quartz with a finite aluminum layer as a function of the frequency-thickness product fh.

curves and their imaginary branches are now dispersive, i.e., they depend explicitly on the frequency-thickness product fh, where h is the metal layer thickness and f the frequency. It is worthwhile noting that there is no partial-wave selection rule problem in the metal since all partial waves are indistinctly retained in the computation. However, the problems encountered with pseudo-surface acoustic waves in Sec. V still remain, though they are connected with the partial-wave selection rule inside the substrate only. Figure 13 displays the imaginary branches of the slowness curves of (YXl)/36 quartz with a finite aluminum layer, as a function of the frequency-thickness product fh.

VII. CONCLUSION

We have obtained the imaginary branches of SAW slowness curves by formulating a plane-wave propagation problem with a complex transverse slowness. In the case of true, i.e., lossless, SAW, it has been shown that the imaginary branches can be obtained by a search in the complex transverse slowness plane as a function of the propagation slowness. For slowness curves such that the slowness in the direction of propagation is maximal on axis, it further turns out that the imaginary branches involve only purely imaginary transverse slownesses. A useful consequence of the approach in this work is that the many modal or spectral methods that have been developed to account for waveguides or diffraction based on the angular spectrum of waves approach can be used unchanged, except for the imaginary branches of slowness curves being exact instead of the result of the parabolic or another approximation. As a side result, the parabolic approximation has been compared with the exact solution and it turns out that its quality depends dramatically on the particular material cut considered. When trying to extend the method to pseudo- or leaky SAW, we have faced difficulties in the process of identifying a solution. These difficulties are twofold, with possible problems in the partial-waves selection or the appearance of amplification rather than attenuation of SAW in the effective permittivity computation. The question of determining imaginary branches for leaky SAW is then left open.

ACKNOWLEDGMENT

The authors are grateful to Alexandre Reinhardt and William Steichen for enlightening discussions.

APPENDIX: PARTIAL-WAVE SELECTION IN THE Π_{13} PLANE

In this appendix, the partial-wave selection rule problem arising in Sec. V is shown to exist on one particular example. We consider the slowness surface for one of the four pairs of partial waves. For real-valued slownesses, this slowness surface is for bulk acoustic waves.[22] We take its equation in the form

$$s_1^2 + s_2^2 + s_3^2 + 2\nu s_2 s_3 = S^2, \tag{A1}$$

where S and ν are constants. This is an homogeneous polynomial of degree 2 in the variables s_1, s_2, and s_3 that would represent a sphere but for the term $\nu s_2 s_3$, where ν can be considered arbitrarily small. The problem is to obtain s_2 with s_1 and s_3 in the Π_{13} plane defined in Sec. V. Setting $s_3 = \epsilon j |s_3|$, with $\epsilon = \pm 1$, the solution of this second degree equation is

$$s_2 = -\epsilon j \nu |s_3| \pm \sqrt{\eta} \quad \text{if } \eta \geqslant 0, \tag{A2}$$

$$s_2 = -\epsilon j \nu |s_3| \pm j\sqrt{|\eta|} \quad \text{if } \eta < 0, \tag{A3}$$

with

$$\eta = S^2 - s_1^2 + (1-\nu^2)|s_3|^2 \tag{A4}$$

It is clear that in the case $\eta \geqslant 0$, the two possible values of s_2 have the same imaginary part, and both will be classified simultaneously as reflected or transmitted depending on ϵ, i.e., on the sign of the imaginary part of s_3. When $\eta < 0$, opposite signs of the imaginary parts are recovered as soon as $|\eta| \geqslant \nu^2$, i.e., if

$$s_1^2 - |s_3|^2 \geqslant S^2. \tag{A5}$$

It can be noticed that this hyperbola shape is consistent with the numerical examples displayed in Figs. 8–12 to describe the shape of the curve limiting the rightmost part of the locus of initially allowed LE SAW solutions.

[1] J. G. Harris, *Linear Elastic Waves* (Cambridge University Press, Cambridge, 2001).
[2] D. Marcuse, *Theory of Dielectric Optical Waveguides* (Academic, Boston, 1991).
[3] T. L. Szabo and J. Slobodnik, IEEE Trans. Sonics Ultrason. **20**, 240 (1973).
[4] M. Tan and C. Flory, IEEE Trans. Ultrason. Ferroelectr. Freq. Control **34**, 93 (1987).
[5] C. Flory and M. Tan, IEEE Trans. Ultrason. Ferroelectr. Freq. Control **35**, 498 (1988).
[6] G. Visintini, A. Baghai-Wadji, and O. Männer, IEEE Trans. Ultrason. Ferroelectr. Freq. Control **39**, 61 (1992).
[7] A. A. Oliner, Proc. IEEE **64**, 615 (1976).
[8] M. Solal, IEEE Trans. Ultrason. Ferroelectr. Freq. Control **50**, 1729 (2003).
[9] M. Jungwirth, N. Pocksteiner, G. Kovacs, and R. Weigel, IEEE Trans. Ultrason. Ferroelectr. Freq. Control **49**, 519 (2002).
[10] A. L. Slobodnik, E. D. Conway, and R. T. Delmonico, *Microwave Acoustic Handbook*, (1A Vol. Air Force Cambridge Research Laboratories, Bedford, Mass., 1973).
[11] V. Laude and S. Ballandras, J. Appl. Phys. **94**, 1235 (2003).
[12] M. G. Cohen, J. Appl. Phys. **38**, 3821 (1967).
[13] G. W. Farnell, Wave Electron. **3**, 207 (1978).
[14] J. K. Knowles, J. Geophys. Res. **71**, 5480 (1966).
[15] D. P. Morgan, *Surface-Wave Devices for Signal Processing* (Elsevier, New York, 1985).
[16] A. H. Fahmy and E. L. Adler, Appl. Phys. Lett. **22**, 495 (1973).

[17]E. L. Adler, IEEE Trans. Ultrason. Ferroelectr. Freq. Control **37**, 485 (1990).
[18]T. Pastureaud, V. Laude, and S. Ballandras, Appl. Phys. Lett. **80**, 2544 (2002).
[19]R. Peach, IEEE Trans. Ultrason. Ferroelectr. Freq. Control **48**, 1308 (2001).
[20]V. Laude, M. Wilm, and S. Ballandras, J. Appl. Phys. **93**, 10084 (2003).
[21]S. Camou, V. Laude, T. Pastureaud, and S. Ballandras, IEEE Trans. Ultrason. Ferroelectr. Freq. Control **50**, 1363 (2003).
[22]B. A. Auld, *Acoustic Fields and Waves in Solids* (Wiley, New York, 1973).